J|A|C|S
ARTICLES

Activation of Dinitrogen by Solid and Liquid Aluminum Nanoclusters: A Combined Experimental and Theoretical Study

Baopeng Cao,[†] Anne K. Starace,[†] Oscar H. Judd,[†] Indrani Bhattacharyya,[†] Martin F. Jarrold,*[†] José M. López,[‡] and Andrés Aguado*[‡]

Chemistry Department, Indiana University, 800 East Kirkwood Avenue, Bloomington, Indiana 47405, and Departamento de Física Teórica, Universidad de Valladolid, Valladolid 47011, Spain

Received April 28, 2010; E-mail: mfj@indiana.edu; aguado@metodos.fam.cie.uva.es

Abstract: Cross sections for chemisorption of N_2 onto $Al_{44}^{+/-}$ cluster ions have been measured as a function of relative kinetic energy and the temperature of the metal cluster. There is a kinetic energy threshold for chemisorption, indicating that it is an activated process. The threshold energies are around 3.5 eV when the clusters are in their solid phase and drop to around 2.5 eV when the clusters melt, indicating that the liquid clusters are much more reactive than the solid. Below the melting temperature the threshold for Al_{44}^{-} is smaller than for Al_{44}^{+}, but for the liquid clusters the anion and cation have similar thresholds. At high cluster temperatures and high collision energies the $Al_{44}N_2^{+/-}$ chemisorption product dissociates through several channels, including loss of Al, N_2, and Al_3N. Density functional calculations are employed to understand the thermodynamics and the dynamics of the reaction. The theoretical results suggest that the lowest energy pathway for activation of dinitrogen is not dynamically accessible under the experimental conditions, so that an explicit account of dynamical effects, via molecular dynamics simulations, is necessary in order to interpret the experimental measurements. The calculations reproduce all of the main features of the experimental results, including the kinetic energy thresholds of the anion and cation and the dissociation energies of the liquid $Al_{44}N_2^{+/-}$ product. The strong increase in reactivity on melting appears to be due to the volume change of melting and to atomic disorder.

Introduction

The properties of metal clusters are often different from those of the corresponding bulk material, and, at least in the small size regime, they can show a strong dependence on cluster size. Substantial size-dependent variations in, for example, the stabilities and geometries of metal clusters and their optical and electronic properties have been well-documented.[1] Recent measurements have shown large, size-dependent fluctuations in the melting temperatures,[2-5] and a substantial effort has been directed toward understanding their origin. The melting temperatures of small metal particles are usually depressed,[6,7] and when this general trend is coupled with the fluctuations, it can lead to melting temperatures that are much lower than those of the bulk for some cluster sizes.

There has also been a lot of interest in the chemical properties of metal clusters.[8-18] Commercial catalysts are usually small metal particles on an oxide support. Isolated metal clusters can display chemical properties that are very different from those of the bulk surfaces, and enormous variations in reaction rates as a function of cluster size have been observed. Chemical reactions are controlled by subtle variations in the size of activation barriers, and understanding the chemical properties of metal clusters is a challenge.

[†] Indiana University.

[‡] Universidad de Valladolid.

(1) De Heer, W. A. *Rev. Mod. Phys.* **1993**, *65*, 611–676.

(2) Schmidt, M.; Kusche, R.; von Issendorff, B.; Haberland, H. *Nature* **1998**, *393*, 238–240.

(3) Schmidt, M.; Haberland, H. *C. R. Phys.* **2002**, *3*, 327–340.

(4) Neal, C. M.; Starace, A. K.; Jarrold, M. F. *Phys. Rev. B* **2007**, *76*, 054113.

(5) Starace, A. K.; Cao, B.; Judd, O. H.; Bhattacharyya, I.; Jarrold, M. F. *J. Chem. Phys.* **2010**, *132*, 034302.

(6) Pawlow, P. *Z. Phys. Chem.* **1909**, *65*, 1–35.

(7) Buffat, Ph.; Borel, J.-P. *Phys. Rev. A* **1976**, *13*, 2287–2298.

(8) Richtsmeier, S. C.; Parks, E. K.; Liu, K.; Pobo, L. G.; Riley, S. J. *J. Chem. Phys.* **1985**, *82*, 3659–3665.

(9) Geusic, M. E.; Morse, M. D.; O'Brien, S. C.; Smalley, R. E. *Rev. Sci. Instrum.* **1985**, *56*, 2123–2130.

(10) Trevor, D. J.; Whetten, R. L.; Cox, D. M.; Kaldor, A. *J. Am. Chem. Soc.* **1985**, *107*, 518–519.

(11) Creegan, K. M.; Jarrold, M. F. *J. Am. Chem. Soc.* **1990**, *112*, 3768–3773.

(12) Jarrold, M. F.; Ijiri, Y.; Ray, U. *J. Chem. Phys.* **1991**, *94*, 3607–3618.

(13) Balteanu, I.; Balaj, O. P.; Beyer, M. K.; Bondybey, V. E. *Int. J. Mass Spectrom.* **2006**, *255*, 71–75.

(14) Wyrwas, R. B.; Yoder, B. L.; Maze, J. T.; Jarrold, C. C. *J. Phys. Chem. A* **2006**, *110*, 2157–2164.

(15) Wyrwas, R. B.; Jarrold, C. C. *J. Am. Chem. Soc.* **2006**, *128*, 13688–13689.

(16) Johnson, G. E.; Tyo, E. C.; Castleman, A. W. *Proc. Natl. Acad. Sci. U.S.A.* **2008**, *105*, 18108–18113.

(17) Citir, M.; Liu, F.; Armentrout, P. B. *J. Chem. Phys.* **2009**, *2009*, 054303.

(18) Xie, Y.; Dong, F.; Heinbuch, S.; Rocca, J. J.; Bernstein, E. R. *Phys. Chem. Chem. Phys.* **2010**, *12*, 947–959.

In this article we describe a combined theoretical and experimental study of the chemisorption of dinitrogen on Al_{44}^+ and Al_{44}^- clusters. The unique feature of these studies is that they have been performed as a function of the cluster temperature over a range that covers both the liquid-like and solid-like phases, which allows us to investigate how the phase affects the chemical reactivity. Not much is known about the chemistry of liquid metal surfaces because the bulk melting temperatures are usually high, and the vapor pressure of most liquid metals makes them difficult to study in a vacuum. The metal clusters studied here have depressed melting temperatures and avoid both of these experimental challenges. The chemistry on a liquid metal cluster may be different from that on the solid. For example, the enhanced mobility of the liquid metal at the atomic level may facilitate the dissolution of adsorbates, enabling different chemical processes to occur.

The activation of N_2 (nitrogen fixation) is a challenge because of the large N_2 bond energy. In nature, the conversion of N_2 into NH_3 is essential for life because fixed nitrogen is required for synthesis of DNA, RNA, and proteins. Abiotic nitrogen fixation (the conversion of N_2 to NO_x) requires high temperature and occurs in lightning and as a side product of combustion. The catalytic conversion of N_2 to NH_3 is an important industrial process. The most common method remains the Haber–Bosch process, which requires both high temperature and pressure.

There have been several previous studies of the general properties of small clusters formed by a mixture of Al and N atoms. For very small clusters like Al_2N_2, a strong dominance of the N–N bond over the Al–N bonds is observed.[19−21] Such a small number of aluminum atoms cannot achieve a full reduction of the nitrogen atoms. The N–N bond length in Al_2N_2 is about 1.25 Å, so it is elongated with respect to its gas phase value of 1.098 Å. This distance is representative of a partial reduction stage associated with the formation of an anion N_2^{2-} moiety rather than separated nitrido (N^{3-}) anions. In a computational study of M_3N_3 clusters (M = Al, Ga, In), Kandalam et al.[22] found a strong tendency to form N–N bonds only for Ga_3N_3 and In_3N_3, while Al_3N_3 has a planar ring structure with only Al–N ionic bonds. Aluminum is therefore a much better reducing agent for nitrogen than Ga and In, because the strength of the metal–nitrogen bond decreases on going from Al to Ga to In, while the strength of the metal–metal bonds increases along the same series. Larger stoichiometric Al_nN_n clusters thus adopt typical ionic-like structures,[23,24] very similar to those adopted by $(MgO)_n$ or alkali halide clusters.[25−28] In the opposite limit of dilute concentrations of nitrogen, the structures of Al_nN clusters (with *n* up to 19) have been studied by several

groups.[29−34] Averkiev et al.[32,33] have combined photoelectron spectroscopy and *ab initio* calculations to show the formation of a N-centered octahedral Al_6N unit in Al_6N^- and Al_7N^- cluster anions. For these small cluster sizes, the nitrogen impurity is therefore absorbed (rather than adsorbed) by the metallic host. According to the *ab initio* calculations of Bai et al.,[34] this tendency of the nitrogen atom to occupy interior positions is maintained only up to *n* = 10. For larger clusters, the nitrogen impurity prefers a peripheral position with just four Al–N bonds, which is the same coordination number as in bulk aluminum nitride.

Cao et al.[35] have recently reported an ion beam study of the reaction of N_2 with Al_{100} cluster cations. The cations are thermalized before colliding with N_2, so that the reaction cross sections and the activation energies for chemisorption of N_2 can be determined as a function of cluster temperature. At the low temperatures at which Al_{100}^+ is solid, an activation energy of 3.50 eV was determined for the formation of the only collision product, $Al_{100}N_2^+$, which is consistent with the idea that the N_2 molecule is chemisorbed on the Al_{100}^+ cluster. For the higher temperatures corresponding to a liquid Al_{100}^+ reactant, the activation barrier dropped by ∼1 eV, implying that the metal cluster is much more reactive in its liquid phase than in its solid phase. In fact, the 1 eV decrease in activation barrier leads to a 10^8-fold increase in the reaction constant at the melting temperature. The higher reactivity of the liquid cluster was tentatively ascribed to the higher mobility of Al atoms, allowing the cluster to adjust better to the incoming N_2 molecule.

Romanowski et al.[36] have performed theoretical studies of the reaction between N_2 and the (111) solid aluminum surface. They find that dissociative chemisorption of N_2 is an exothermic reaction with an activation barrier of 3.0 eV. But to the best of our knowledge, there are no theoretical calculations on the reactions of N_2 with aluminum clusters, either solid or liquid. Very recently, Roy et al.[37] have modeled the activation of dinitrogen by solid Li_n clusters with *n* = 2, 4, 6, and 8. Li_8 is found to be the smallest cluster able to cleave the triple bond of the N_2 molecule completely in a highly exothermic process. Smaller clusters achieve only a partial reduction of dinitrogen: for example, in Li_4N_2, the N–N bond is elongated to about 1.25 Å, which is characteristic of a N_2^{2-} moiety where the triple bond has been reduced to a double bond. Similarly, in Li_6N_2, the N–N distance is further elongated to about 1.49 Å, which reveals the formation of a "hydrazido" complex with a single bond between the two nitrogen atoms. The structure of Li_8N_2 contains two nitrido N^{3-} anions and is very similar to the Na_9O_2 molecule recently identified in a study of oxygen-doped sodium clusters.[38,39] This suggests some similarities in the adsorption behavior of

(19) Boo, B. H.; Liu, Z. *J. Phys. Chem. A* **1999**, *103*, 1250–1254.
(20) Andrews, L.; Zhou, M.; Chertihin, G. V.; Bare, W. D.; Hannachi, Y. *J. Phys. Chem. A* **2000**, *104*, 1656–1661.
(21) Kandalam, A. K.; Pandey, R.; Blanco, M. A.; Costales, A.; Recio, J. M.; Newsam, J. M. *J. Phys. Chem. B* **2000**, *104*, 4361.
(22) Kandalam, A. K.; Blanco, M. A.; Pandey, R. *J. Phys. Chem. B* **2001**, *105*, 6080.
(23) Kandalam, A. K.; Blanco, M. A.; Pandey, R. *J. Phys. Chem. B* **2002**, *106*, 1945.
(24) Costales, A.; Blanco, M. A.; Francisco, E.; Martín Pendás, A.; Pandey, R. *J. Phys. Chem. B* **2006**, *110*, 4092.
(25) Aguado, A.; Ayuela, A.; López, J. M.; Alonso, J. A. *Phys. Rev. B* **1998**, *58*, 9972.
(26) Aguado, A.; Ayuela, A.; López, J. M.; Alonso, J. A. *J. Phys. Chem. B* **1997**, *101*, 5944.
(27) Aguado, A.; López-Gejo, F.; López, J. M. *J. Chem. Phys.* **1999**, *110*, 4788.
(28) Aguado, A.; López, J. M. *J. Phys. Chem. B* **2000**, *104*, 8398.

(29) Nayak, S. K.; Khanna, S. N.; Jena, P. *Phys. Rev. B* **1998**, *57*, 3787.
(30) Wang, B.; Zhao, J.; Shi, D.; Chen, X.; Wang, G. *Phys. Rev. A* **2005**, *72*, 023204.
(31) Guo, L.; Wu, H.-S. *Int. J. Quantum Chem.* **2006**, *106*, 1250.
(32) Averkiev, B. B.; Boldyrev, A. I.; Li, X.; Wang, L.-S. *J. Phys. Chem. A* **2007**, *111*, 34.
(33) Averkiev, B. B.; Call, S.; Boldyrev, A. I.; Wang, L.-M.; Huang, W.; Wang, L.-S. *J. Phys. Chem. A* **2008**, *112*, 1873.
(34) Bai, Q.; Song, B.; Hou, J.; He, P. *Phys. Lett. A* **2008**, *372*, 4545, and references therein.
(35) Cao, B.; Starace, A. K.; Judd, O. H.; Jarrold, M. F. *J. Am. Chem. Soc.* **2009**, *131*, 2446.
(36) Romanowski, Z.; Krukowski, S.; Grzegory, I.; Porowski, S. *J. Chem. Phys.* **2001**, *114*, 6353.
(37) Roy, D.; Navarro-Vázquez, A.; Schleyer, P. v. R. *J. Am. Chem. Soc.* **2009**, *131*, 13045.
(38) Hock, C.; Strassburg, S.; Haberland, H.; Issendorff, B. v.; Aguado, A.; Schmidt, M. *Phys. Rev. Lett.* **2008**, *101*, 023401.

N_2 and O_2 on metals. Roach et al.[40] have reported a combined experimental and theoretical study of the reactions of aluminum cluster anions with water. For some clusters, like Al_{16}^-, Al_{17}^-, and Al_{18}^-, dissociative chemisorption of water results in the production of H_2. Also, Henry et al.[41,42] have modeled the disociative chemisorption of molecular hydrogen on charged and neutral aluminum clusters. A general perspective on the importance of clusters as model systems for investigating nanoscale catalysis through combined experimental and theoretical efforts has been recently provided by Johnson et al.[43]

The main motivations for this work are to analyze the influences of thermodynamic phase and cluster charge on the activation of dinitrogen by aluminum clusters and to provide a detailed microscopic interpretation of the underlying collision and reaction dynamics. We have chosen aluminum cluster ions with 44 atoms (which is smaller than the Al_{100}^+ cluster previously studied[35]) because they are sufficiently small that computer simulations can be performed at a reasonable cost, and at the same time both Al_{44}^+ and Al_{44}^- show a well-defined melting transition with a low melting temperature. Smaller Al clusters genearlly have broad and ill-defined melting transitions, so the sensitivity of the reaction rates across the melting transition is more difficult to study. A low melting temperature is also desirable for possible applications in low-temperature chemical reactivity. Finally, we have previously found[44,45] that both Al_{44}^+ and Al_{44}^- adopt a highly symmetric and compact structure, which dramatically reduces the number of different possible isomers for $Al_{44}N_2^+$ and $Al_{44}N_2^-$. Moreover, the global minimum (GM) structure is well separated in energy from all metastable atomic configurations, so we can reliably study the interaction of N_2 with a solid cluster of well-defined geometry, instead of the more complex case of a mixture of isomers.

Experimental Methods

The experimental apparatus used to study the reactions between aluminum clusters and N_2 is similar to that recently used to measure the heat capacities for aluminum clusters.[46] Here we provide a brief description of the experimental apparatus, only dwelling on the changes made to enable the reactivity studies. The aluminum clusters are generated by pulsed laser vaporization of a liquid aluminum target in a continuous flow of helium buffer gas.[47] The clusters are carried by the buffer gas flow from the source region, where they are guided into a 10 cm long temperature-variable extension, where their temperature is set by equilibration with the walls of the extension through collisions with the buffer gas. The temperature is regulated to better than ± 2 K by a programmable temperature/process controller. Measurements indicate that the clusters achieve thermal equilibrium with the walls of the extension.[46] The cluster ions that exit the temperature-variable extension are focused into a quadrupole mass spectrometer set to transmit a single cluster size. The size-selected clusters are focused into an ion beam and directed through a low-pressure reaction cell containing nitrogen gas. The pressure of the nitrogen was kept sufficiently low (less than 1 mTorr) that the clusters experience only around one collision, on average, as they travel through the reaction cell. This is important because unreactive collisions can excite the cluster ions so that their internal energy distribution is no longer characteristic of the temperature set in the temperature-variable extension. The ion energy in the collision cell was determined from the voltage difference between the reaction cell and the temperature-variable extension. The ion energy was not directly measured because, for the reaction studied here, the center of mass collision energy is a small fraction of the ion's laboratory energy (the ion is much heavier than the N_2). The product ions and unreacted cluster ions that exit the reaction cell are focused into a second quadrupole mass spectrometer, where they are analyzed and then detected by an off-axis collision dynode and dual microchannel plates.

Experimental Results

A number of products were detected from the interaction between $Al_{44}^{+/-}$ and N_2, their relative abundances depending on the cluster temperature and the relative kinetic energy. Figure 1 shows the cross sections for formation of the significant products plotted against relative kinetic energy for the Al_{44}^+ cation reaction with N_2. The results shown in the figure are typical individual data sets at initial cluster temperatures of 558, 758, 908, and 1058 K. At 558 K, $Al_{44}N_2^+$ is the dominant product. The $Al_{44}N_2^+$ product must result from chemisorption of N_2 because an $Al_{44}^+-N_2$ complex with a weakly bound, physisorbed N_2 would not survive to such a high temperature. Results for temperatures below 558 K, down to 258 K, are similar to those shown in the figure for 558 K. There is a kinetic energy threshold for the $Al_{44}N_2^+$ product around 3 eV: the cross section increases with increasing kinetic energy and then starts to plateau around 8 eV. A small amount of a secondary product labeled $Al_{42}N_2^+$ (purple points and line) is detected at the higher collision energies. We discuss the nature and origin of this product further below.

The Al_{44}^+ cluster has a peak in its heat capacity centered around 658 K which is attributed to melting (see below). So at 558 K this cluster is solid-like, and at 758 K (the second temperature in Figure 1) it is liquid-like. At 758 K, the dominant product from the reaction with N_2 is still $Al_{44}N_2^+$. However, the threshold occurs at a significantly lower kinetic energy, closer to 2 eV than to 3 eV, and the cross sections for the $Al_{44}N_2^+$ product peak around 6 eV and then decrease. There is a sharp increase in the amount of the product labeled $Al_{42}N_2^+$ at the highest kinetic energies, and several other products appear in significant quantities at the higher collision energies for this temperature. $Al_{41}N^+$ (dark blue points and line) is the most abundant secondary product after $Al_{42}N_2^+$. The decrease in the cross sections for $Al_{44}N_2^+$ at high collision energies suggests that a substantial amount of the chemisorption product reacts further to form secondary products. However, the amount of secondary products found at high collision energies is insufficient to account for the drop in the $Al_{44}N_2^+$ cross sections, suggesting that another unobserved product is being formed. One explanation for this observation is that the $Al_{44}N_2^+$ product becomes sufficiently energized at high collision energies that it simply dissociates back to the reactants:
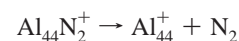
$$Al_{44}N_2^+ \rightarrow Al_{44}^+ + N_2$$

Another possible explanation is that the $Al_{44}N_2^+$ complex loses an aluminum atom:

(39) Majer, K.; Hock, C.; Issendorff, B. v.; Aguado, A. *J. Chem. Phys.* **2009**, *131*, 204313.
(40) Roach, P. J.; Woodward, W. H.; Castleman, A. W., Jr.; Reber, A. C.; Khanna, S. N. *Science* **2009**, *323*, 492.
(41) Henry, D. J.; Yarousky, I. *J. Phys. Chem. A* **2009**, *113*, 2565.
(42) Henry, D. J.; Varano, A.; Yarousky, I. *J. Phys. Chem. A* **2009**, *113*, 5832.
(43) Johnson, G. E.; Mitrić, R.; Bonačić-Koutecký, V.; Castleman, A. W., Jr. *Chem. Phys. Lett.* **2009**, *475*, 1.
(44) Starace, A. K.; Neal, C. M.; Cao, B.; Jarrold, M. F.; Aguado, A.; López, J. M. *J. Chem. Phys.* **2008**, *129*, 144702.
(45) Starace, A. K.; Neal, C. M.; Cao, B.; Jarrold, M. F.; Aguado, A.; López, J. M. *J. Chem. Phys.* **2009**, *131*, 044307.
(46) Neal, C. M.; Starace, A. K.; Jarrold, M. F. *J. Am. Soc. Mass Spectrom.* **2007**, *18*, 74–81.
(47) Neal, C. M.; Breaux, G. A.; Cao, B.; Starace, A. K.; Jarrold, M. F. *Rev. Sci. Instrum.* **2007**, *78*, 075108.
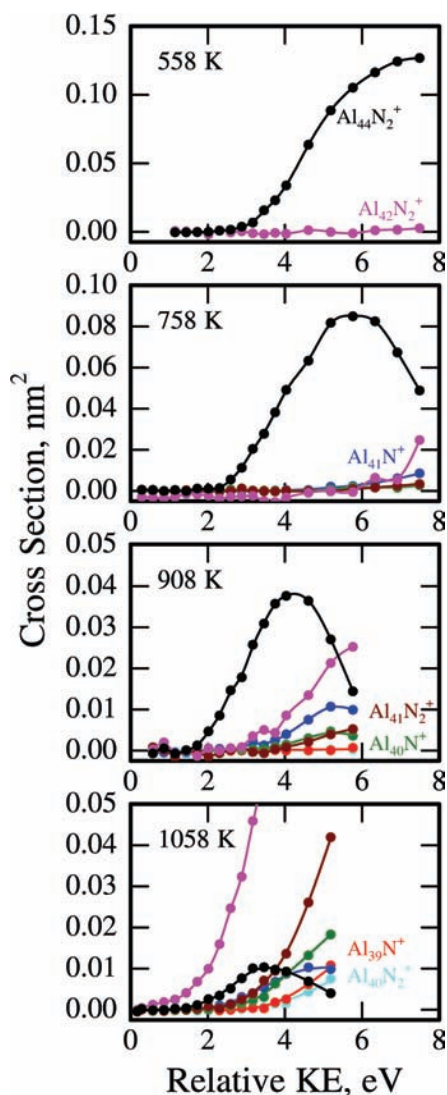
Figure 1. Cross sections for the formation of the main products observed from the reaction of Al_{44}^+ with N_2, plotted against relative kinetic energy at four representative temperatures. The data points and lines are color coded to the labels shown to the right of the plots. The product labeled $Al_{42}N_2^+$ is a mixture of $Al_{42}N_2^+$ and Al_{43}^+ (which differ in mass by 1 Da). Similarly, $Al_{41}N_2^+$ is a mixture of $Al_{41}N_2^+$ and Al_{42}^+, and $Al_{40}N_2^+$ is a mixture of $Al_{40}N_2^+$ and Al_{41}^+.

$$Al_{44}N_2^+ \rightarrow Al_{43}N_2^+ + Al$$

The resulting $Al_{43}N_2^+$ ion has an m/z ratio that is 1 Da larger than that of the Al_{44}^+ reactant. With our experimental configuration, it is not possible to resolve a small amount of $Al_{43}N_2^+$ product in the presence of the much more abundant Al_{44}^+ reactant, so the presence of this product cannot be directly confirmed.

$Al_{42}N_2^+$ and Al_{43}^+ are also separated by 1 Da, and we were unable to resolve these products as well. However, the center of the combined peak lies between the masses expected for $Al_{42}N_2^+$ and Al_{43}^+, suggesting that both products contribute. Based on the position of the center of the peak, it appears that there is more $Al_{42}N_2^+$ present than Al_{43}^+ under most conditions, which is why the combined product is labeled $Al_{42}N_2^+$ in Figure 1. The observation of $Al_{42}N_2^+$ suggests that the main product from the initial dissociation of $Al_{44}N_2^+$ is $Al_{43}N_2^+$; i.e., dissociation of $Al_{44}N_2^+$ occurs mainly through the following sequence:

$$Al_{44}N_2^+ \rightarrow Al_{43}N_2^+ + Al \rightarrow Al_{42}N_2^+ + 2Al$$
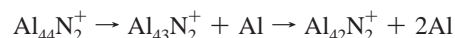
The Al_{43}^+ product mentioned above could result from collision-induced dissociation of the Al_{44}^+ reactant:

$$Al_{44}^+ + N_2 \rightarrow Al_{43}^+ + Al + N_2$$

or from loss of N_2 from $Al_{43}N_2^+$. Collision-induced dissociation is expected to occur by a two-step process: first the collision with the N_2 transfers some of the relative kinetic energy into internal energy of the cluster, and then the energized Al_{44}^+ subsequently dissociates (if it has enough energy). In the collisional activation step, a distribution of energies from zero up to the collision energy is transferred into internal energy. This is different from reactive collisions (chemisorption), where all of the relative kinetic energy must be converted into internal energy (potential + vibrational). Dissociation of the energized Al_{44}^+ occurs through a statistical unimolecular reaction. Dissociation of energized reaction products (i.e., $Al_{44}N_2^+$) occurs through the same process. Al_{44}^+ and $Al_{44}N_2^+$ are relatively large species, and their unimolecular dissociation will occur with a substantial kinetic shift. Thus, an internal energy considerably in excess of the Al_{43}^+−Al bond energy is required to drive dissociation on the experimental time scale.

Loss of AlN_2 from $Al_{44}N_2^+$ can be ruled out as the source of the Al_{43}^+ product because, according to calculations, $Al−N_2$ is a van der Waals molecule (bound by around 16 kJ/mol) and $NAlN$ is higher in energy than $Al + N_2$ by around 500 kJ/mol.[20] The $Al_{41}N^+$ product mentioned above probably results from a secondary reaction of the $Al_{44}N_2^+$ chemisorption product:

$$Al_{44}N_2^+ \rightarrow Al_{41}N^+ + Al_3N$$

Al_3N is known to be a stable aluminum/nitrogen cluster.[19,48] Incidently, observation of the $Al_{41}N^+$ product shows that the N_2 is dissociatively chemisorbed.

At a cluster temperature of 908 K, $Al_{44}N_2^+$ remains the dominant product at low collision energies (see Figure 1), but the plateau and falloff in the cross sections for this product now occur at lower collision energies. The threshold for the $Al_{44}N_2^+$ product is at a slightly lower kinetic energy than at 758 K. However, the thresholds for the secondary products have moved to significantly lower kinetic energies. In addition, more secondary products are observed and are identified in Figure 1: $Al_{41}N_2^+$ (brown points and line) and $Al_{40}N^+$ (green points and line) are both observed at this temperature, though their cross sections are less than 0.01 nm². The product labeled $Al_{41}N_2^+$ is a mixture of $Al_{41}N_2^+$ and Al_{42}^+ (which differ in mass by 1 Da and are unresolved in the mass spectrum). The $Al_{41}N_2^+$ and Al_{42}^+ products could result from loss of an Al atom from $Al_{42}N_2^+$ and Al_{43}^+, respectively. The Al_{42}^+ could also result from loss of Al_2N_2 from $Al_{44}N_2^+$. According to calculations,[20] AlN_2Al is bound by 176 kJ/mol with respect to dissociation according to

$$AlN_2Al \rightarrow Al + N_2 + Al$$

The $Al_{40}N^+$ product could result from loss of Al_4N from the $Al_{44}N_2^+$ product or from loss of an aluminum atom from $Al_{41}N^+$.

At a cluster temperature of 1058 K, the thresholds to what were the secondary products at lower temperature continue to shift to lower collision energies, so that the $Al_{42}N_2^+/Al_{43}^+$ product

(48) Leskiw, B. D.; Castleman, A. W.; Ashman, C.; Khanna, S. N. *J. Chem. Phys.* **2001**, *114*, 1165−1169.

(labeled $Al_{42}N_2^+$ in Figure 1) has the lowest kinetic energy threshold. $Al_{42}N_2^+/Al_{43}^+$ is also the most abundant product at 1058 K. The threshold for the $Al_{44}N_2^+$ product occurs at approximately the same kinetic energy as at 908 K; however, the cross sections plateau and peak at a lower kinetic energy and the peak cross sections are much smaller than at a cluster temperature of 908 K. More secondary products emerge at this higher temperature: specifically, $Al_{40}N_2^+/Al_{41}^+$ (light blue points and line labeled $Al_{40}N_2^+$ in Figure 1) and $Al_{39}N^+$ (red points and line) become significant.

The products observed for the reaction between Al_{44}^- and N_2 are virtually identical to those reported above for the reaction of the Al_{44} cation. The product abundances for the Al_{44} anion and cation have similar dependencies on relative kinetic energy and cluster temperature, and so we do not show the results for the Al_{44} anion here.

Analysis of the Experimental Results

The main product observed at all but the highest cluster temperatures and relative kinetic energies is $Al_{44}N_2^{+/-}$, which results from chemisorption of the N_2 onto the cluster. This reaction shows a kinetic energy threshold, indicating that there is an activation barrier. If the internal degrees of freedom for the reactants were unexcited, the kinetic energy threshold would provide an upper limit to this barrier. The barrier may be smaller than the measured threshold because of dynamic effects, where the lowest energy pathway is not accessible at the relative kinetic energies required for the reaction to occur (this behavior is found in the simulations described below). The kinetic energy threshold for chemisorption of N_2 on $Al_{44}N_2^{+/-}$ is broadened by the distribution of collision energies that results from the spread in the kinetic energy of the ion beam and from the thermal motion of the nitrogen target gas. Because the mass of the ion is much greater than the mass of the target, in the present case the dominant contribution to threshold broadening comes from the thermal motion of the target, and the contribution from the spread in the ion beam energy can be safely neglected. To determine the true kinetic energy threshold, the measured cross sections are fit with an assumed function which is broadened to account for the thermal motion of the target gas molecules. The function used here is

$$\sigma(E) = \sigma_0 \frac{(E - E_0)^n}{E} \int dE_T\, P(E_T) \exp[-k(E_T + E + D(N_2), D(Al))t] \quad (1)$$

The part of this expression before the integral is the widely used empirical cross section function, where σ_0 is the cross section scaling factor, E is the relative kinetic energy, E_0 is the kinetic energy threshold of the reaction, and n is an adjustable parameter.[49] With $n = 1$, the cross section function corresponds to the simple line of centers model.[50] Note that the cross section function does not incorporate any dependence on the internal energy (we discuss this issue further below). The integral in eq 1 accounts for the dissociation of the $Al_{44}N_2^{+/-}$ product when it is highly excited. This causes the falloff in the cross sections for the $Al_{44}N_2^{+/-}$ product at high temperatures and high collision energies. According to the calculations described below, the $Al_{43}N_2^+ + Al$ products are slightly higher in energy than Al_{44}^+

(49) Armentrout, P. B. *Int. J. Mass Spectrom.* **2000**, *200*, 219–241.
(50) Levine, R. D.; Bernstein, R. B. *Molecular Reaction Dynamics*; Oxford University Press: New York, 1974; p 46.
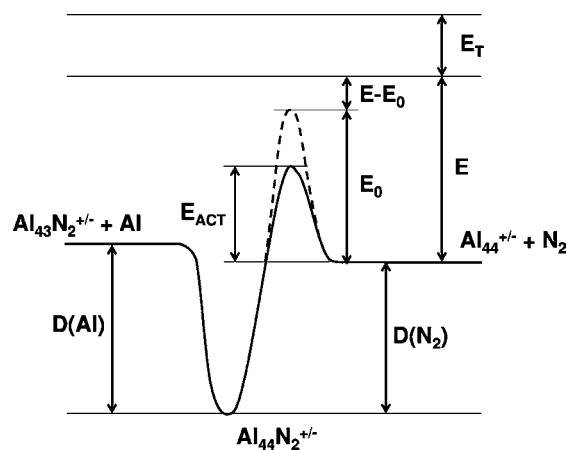
Figure 2. Schematic diagram showing the relation between the different energetic terms appearing in eq 1. E is the relative kinetic energy, E_T is the internal energy of the $Al_{44}^{+/-}$ cluster, E_0 is the kinetic energy threshold, E_{ACT} is the activation energy for the reaction (the highest point on the lowest energy route between reactants and products), and finally, $D(Al)$ and $D(N_2)$ are the dissociation energies of the $Al_{44}N_2^+$ product by loss of Al and N_2, respectively.

$+ N_2$. However, there is a significant energy barrier to loss of N_2 from $Al_{44}N_2^+$ (see below), and so the lowest energy dissociation pathway of $Al_{44}N_2^+$ is probably loss of an Al atom. This is illustrated schematically in Figure 2.

A falloff in the reaction cross sections due to product dissociation has been seen for a number of reactions, and the approach to modeling the behavior used here is similar to those used previously.[51−56] $k(E_T + E + D(N_2),D(Al))$ in eq 1 is the rate constant for dissociation of the $Al_{44}N_2^{+/-}$ product to give $Al_{43}N_2^{+/-} + Al$. $E_T + E + D(N_2)$ is the total internal energy of the $Al_{44}N_2^{+/-}$ product, and $D(Al)$ is the dissociation energy for loss of an Al atom. $D(N_2)$ is the dissociation energy of $Al_{44}N_2^{+/-}$ to yield $Al_{44}^{+/-}$ and N_2, and E_T is the internal energy of the cluster before its collision with an N_2 molecule. E_T is related to the initial temperature of the cluster (i.e., the temperature of the temperature-variable extension). The rate constants were estimated using the quantum RRK model.[57] Note that the rate constant depends on both $D(Al)$ and $D(N_2)$.

To fit the assumed cross section function to the measured cross sections, it must be averaged over the distribution of collision energies that result from the thermal motion of the target gas. This is accomplished using a procedure where the speed and direction of the nitrogen molecule are selected randomly, but with a probability given by the Maxwell–Boltzmann velocity distribution. Averaging over 1000 randomly selected vectors was found to be sufficient. There are five variables in eq 1 that can be adjusted to fit to the measured cross sections: σ_0, E_0, $D(Al)$, $D(N_2)$, and n. The first four were adjusted automatically using a least-squares procedure, while n was adjusted manually. The value of n was varied in increments of 0.25, starting at 0.75 and going up to 2.50. For

(51) Weber, M. E.; Elkind, J. L.; Armentrout, P. B. *J. Chem. Phys.* **1986**, *84*, 1521–1529.
(52) Elkind, J. L.; Armentrout, P. B. *J. Phys. Chem.* **1986**, *90*, 6576–6586.
(53) Liu, F.; Liyanage, R.; Armentrout, P. B. *J. Chem. Phys.* **2002**, *117*, 132–141.
(54) Tan, L.; Liu, F.; Armentrout, P. B. *J. Chem. Phys.* **2006**, *124*, 084302.
(55) Liu, F.; Li, M. L.; Tan, L.; Armentrout, P. B. *J. Chem. Phys.* **2008**, *128*, 194313.
(56) Citir, M.; Liu, F.; Armentrout, P. B. *J. Chem. Phys.* **2009**, *130*, 054309.
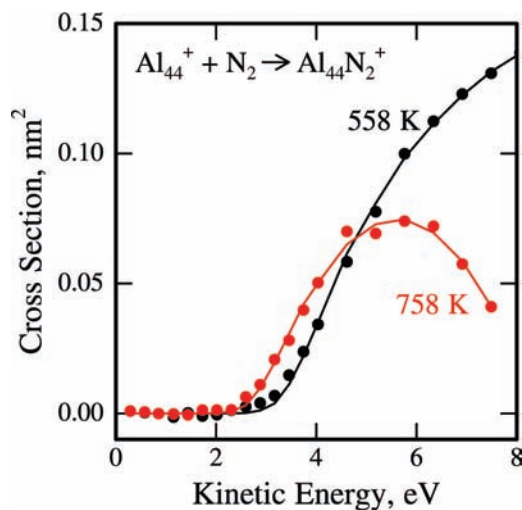(57) Rice, O. K.; Ramsperger, H. C. *J. Am. Chem. Soc.* **1928**, *50*, 617.

Figure 3. Examples of fits of eq 1 to the measured cross sections. The filled points are the experimental results at 558 (black) and 758 K (red), plotted against the relative kinetic energy. The solid lines show the fit to the measured cross sections using eq 1. Both sets of results are well-fit, including the roll-over in the cross sections that occurs at the higher relative kinetic energies for the 758 K data set.

Figure 4. Heat capacities recorded for Al_{44}^+ and Al_{44}^- as a function of temperature (upper half) (data taken from refs 4, 45, and 58). The peaks around 600 K are due to melting transitions. Average kinetic energy thresholds for chemisorption of N_2 on Al_{44}^+ and Al_{44}^- plotted against temperature (lower half). The filled points show thresholds obtained from the best overall fit to the experimental results. Below the melting temperature the best overall fit was obtained with $n = 1.0$. Above the melting temperature the best overall fit was obtained with $n = 1.5$. The open points show the values obtained for the thresholds above the melting temperature with $n = 1.0$.

both the anion and the cation, the best overall fit for temperatures below the melting temperature was obtained with $n = 1.00$. Above the melting temperature, a slightly larger value, $n = 1.50$, gave the best overall fit. Below the melting temperature, the preference for $n = 1.00$ is strong (i.e., the fits degrade quickly as n moves away from 1.00). Above the melting temperature, the preference for $n = 1.50$ is softer, probably because product dissociation is much more important above the melting temperature, and dissociation obscures the kinetic energy dependence of the cross section function.

Examples of the fits are shown in Figure 3, where results are shown for the Al_{44} cation reaction at 558 K (just below the melting transition) and 758 K (which is just above). The cross sections at both temperatures are well fit by the simulation. The threshold for the formation of $Al_{44}N_2^+$ is significantly lower at 758 K than at 558 K. The roll-over in the cross sections at higher kinetic energies in the 758 K data set (which results from dissociation of the $Al_{44}N_2^+$ product when it is highly excited) is also well-fit by the simulation. The fit to the roll-over provides values for $D(Al)$ and $D(N_2)$. These quantities are defined most accurately for temperatures between 750 and 950 K. In this temperature range, the roll-over in the cross sections occurs at a collision energy that is low enough to be in the range we investigated, but not so low that the chemisorption product is severely depleted and only seen over a narrow range of collision energies. Within the 750–950 K temperature range, the average value for $D(Al)$ for the cation is 2.64 eV. The individual $D(Al)$ values in this temperature range are almost identical; the standard deviation of the 13 determinations is 0.02 eV. The results for the anion are almost identical. The average $D(Al)$ for the anion is 2.67 eV, and the standard deviation is also 0.02 eV. The values for $D(N_2)$ are less well defined. For the cation the average value is 2.37 eV and the standard deviation is 0.25 eV, while for the anion the average value is 2.46 eV and the standard deviation is 0.31 eV. The values for $D(Al)$ and $D(N_2)$ reported above are for the dissociation of a liquid $Al_{44}N_2^{+/-}$ cluster to give (presumably) liquid products. Below the $Al_{44}^{+/-}$ melting temperature, the values for $D(Al)$ and $D(N_2)$ deduced from fitting the cross sections fluctuatate widely because the
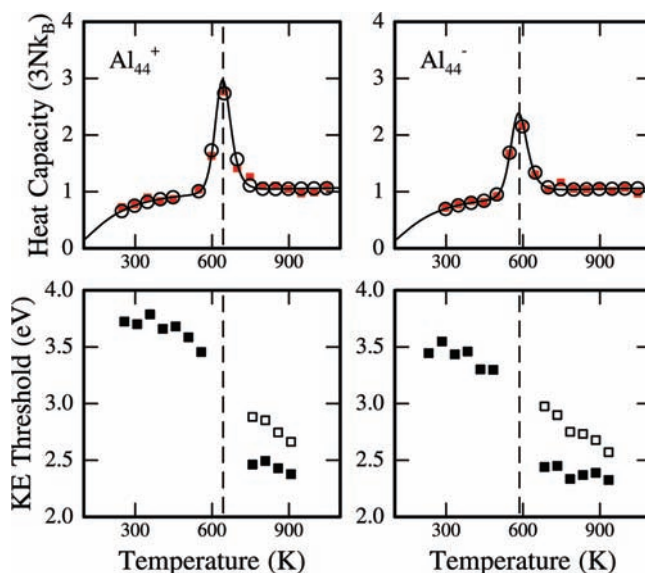
roll-over is not prominent and does not provide enough information to define the dissociation energies.

The lower half of Figure 4 shows plots of the average kinetic energy thresholds determined as a function of temperature for the chemisorption of N_2 on the Al_{44} anion and cation. The average kinetic energy thresholds were determined from 2–4 independent measurements at each temperature. The upper half of Figure 4 shows the heat capacities recorded for Al_{44}^+ and Al_{44}^- as a function of temperature.[4,45] There are peaks in the heat capacities of both the anion and the cation around 600 K which have been attributed to melting transitions. The vertical dashed line shows the center of the melting transition. The anion has a slightly lower melting temperature than the cation. From Figure 4 we can see that below the melting temperature the average kinetic energy thresholds vary only slightly with cluster temperature, decreasing slightly as the temperature is raised.

As described above, the best overall fit to the cross sections for clusters below the melting temperature was obtained with $n = 1.0$. Above the melting temperature, the best overall fit was obtained with $n = 1.5$. The average values obtained in this way are represented by the filled black squares in the lower half of Figure 4. The open squares show the results obtained using $n = 1.0$ for the temperatures above the melting transition. Clearly the change in the value of n used to fit the cross section data causes a significant change in the value of the kinetic energy threshold. Increasing n from 1.0 to 1.5 amplifies the decrease in the kinetic energy thresholds that occurs at the melting transition. Above the melting temperature, the average kinetic energy thresholds for the cation and anion are similar, regardless of the model used to fit the cross section data. Below the melting temperature, the thresholds are much less sensitive to the value

(58) Neal, C. M.; Starace, A. K.; Jarrold, M. F.; Joshi, K.; Krishnamurty, S.; Kanhere, D. G. *J. Phys. Chem. C* **2007**, *111*, 17788.

of *n* than above. The value of *D*(Al) deduced from the fit is insensitive to the value of *n*. However, $D(N_2)$ (which is not as strongly defined by the fits as *D*(Al)) shows some dependence on the value of *n* used in the fit.

In the empirical cross section function used to fit the results (the part of eq 1 before the integral), we ignore the internal energy of the cluster. Is this assumption correct? If we were studying the reaction between an atom and a diatomic molecule (A + BC → AB + C), we would expect that vibrational excitation of the diatomic molecule would lower the activation energy for the reaction. On the other hand, if we consider a surface reaction between a molecule and a bulk object, it is obvious that *all* of the internal energy of the bulk object will not contribute to lowering the activation barrier. In the present case, the internal energy of the $Al_{44}^{+/-}$ increases by around 1 eV per 100 K (based on a modified Debye model for the heat capacity of the cluster[59]). Thus, over the temperature range studied here (around 300−900 K), the internal energy increases by 6 eV. If all of this energy contributed to lowering the activation barrier, it would vanish. At the other extreme, one could argue that only the internal energy of one degree of freedom (the reaction coordinate) should contribute to lowering of the activation barrier. If this is the case, the activation barrier should decrease by around 0.05 eV over a 600 K temperature range. From Figure 4, the kinetic energy thresholds decrease by around 0.2−0.3 eV from just below 300 K to just below 600 K. Some of this decrease may be a direct consequence of the internal energy lowering the activation barrier. The calculations below shed more light on this issue.

While only a small fraction of the internal energy of the cluster plays a role in the chemisorption of N_2, all of the internal energy is expected to play a role in driving the subsequent dissociation of the $Al_{44}N_2^{+/-}$ product because this occurs through a statistical unimolecular reaction. For a system the size of $Al_{44}N_2^{+/-}$ (or $Al_{44}^{+/-}$), there is expected to be a substantial kinetic shift, and the reaction will not occur close to the threshold on the experimental time scale. This is why the subsequent dissociation of the $Al_{44}N_2^{+/-}$ product (or collisionally excited $Al_{44}^{+/-}$) only becomes important at elevated cluster temperatures and elevated kinetic energies.

Computational Methods

All calculations were performed at the Kohn−Sham DFT[60] level by employing the SIESTA code.[61] The detailed computational settings, including the basis set and exchange-correlation functional employed, are offered in the Supporting Information, together with some benchmark calculations.

The first set of calculations involve the unconstrained optimization of the structures of $Al_{44}N^{+/-}$, $Al_{44}N_2^{+/-}$, and $Al_{43}N_2^{+/-}$. Next, the collision process is modeled through both static and dynamic calculations. The dynamic calculations are done using constant-energy Born−Oppenheimer molecular dynamics (BOMD) runs. The aim of these calculations is to mimic as closely as possible the experimental conditions for the chemisorption reaction. The aluminum cluster is first separately thermalized at several temperatures between 400 and 1000 K. The thermalization is done using constant-temperature BOMD with a time step of 3 fs. Next, the N_2 molecule is positioned far from the cluster and endowed with a relative velocity of 4600 m/s, which yields a center-of-mass collision energy of 3.1 eV. This center-of-mass collision energy is similar
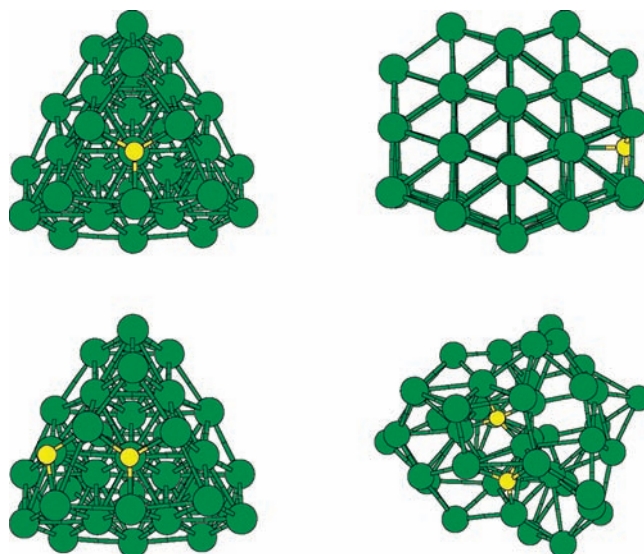
(59) Bohr, J. *Int. J. Quantum Chem.* **2001**, *84*, 249.
(60) Kohn, W.; Sham, L. J. *Phys. Rev.* **1965**, *140*, 1133.
(61) Soler, J. M.; Artacho, E.; Gale, J. D.; García, A.; Junquera, J.; Ordejón, P.; Sánchez-Portal, D. *J. Phys.: Condens. Matter* **2002**, *14*, 2745.

Figure 5. Top row: two different views of the putative global minimum (GM) structure of $Al_{44}N^+$. The three-fold rotation axis and mirror symmetry plane of the host Al_{44}^+ cluster (with D_{3h} point group) can be easily appreciated in the left and right views, respectively. Bottom left: the putative GM structure of $Al_{44}N_2^+$. Bottom right: a snapshot of the liquid structure of $Al_{44}N_2^+$, extracted from a constant-temperature simulation at 900 K.

to the kinetic energy threshold for the chemisorption reaction found in the experiments. Once the ion beam leaves the thermalization chamber, each cluster ion is approximately an isolated system, so the collision process is then followed at constant total energy with a time step of 0.1−0.3 fs. Such short time steps were needed to satisfy the energy conservation requirement due to the high collision velocity and made the *ab initio* MD runs quite expensive. The significant computational expense implies in practice that we cannot afford to do a large number of runs (considering, for example, many different cluster−molecule relative orientations), so we cannot extract meaningful statistical averages for the activation energies, for example. However, we were able to exploit again the high symmetry of the cluster reactant to simulate the collision of N_2 with all different surface facets of the cluster, and the results were very similar. In what follows we will concentrate on the collision of N_2 with a fixed surface facet of the aluminum cluster. The N_2 molecule was oriented both parallel and perpendicular to that cluster surface.

The static calculations are done by constrained geometry optimizations, where some degrees of freedom of the cluster−molecule system are optimized while the others are kept fixed during the optimization. We employed an internal coordinate or Z-matrix representation to express the constraints. If only one degree of freedom is fixed (typically the height of the N_2 molecule with respect to the surface of the aluminum cluster), this method will locate a true transition state, as can be checked by a vibrational analysis. However, in order to best mimic the experimental collision process (which involves collision energies of 3.4 eV at typical threshold conditions) through static calculations, we have found that more contraints are needed (see next sections for details). In this case the path with the lowest possible energy barrier will not be located, but the calculations will give a more realistic description of the barriers surmounted under the conditions of the collision experiment.

Computational Results

1. Structures of Doped Clusters and Reaction Energies. The optimized putative global minimum (GM) structures of $Al_{44}N^+$ and $Al_{44}N_2^+$ are shown in Figure 5. The corresponding anion structures are the same, so they are not shown explicitly. The

single impurity in $Al_{44}N^+$ occupies a high-symmetry position at the cluster surface, which preserves the three-fold rotational symmetry axis of the parent cluster. It is almost exactly incorporated into the surface plane, so it is on the border between adsorption and absorption. The best isomer obtained by incorporating the impurity into a more internal octahedral interstice is 0.9 eV less stable than the putative GM, so the preference for surface locations is clear and agrees with the conclusions given by Bai et al.[34] for clusters with more than 10 Al atoms. In the GM structure, the impurity is coordinated to four Al atoms, as in the stable wurtzite phase of the AlN crystal. The Al–N bond lengths are 1.93 Å for the three in-plane bonds and 2.05 Å for the bond with the internal Al atom, which are still longer than the bulk value of 1.89 Å.[63] The reason for the two different sets of Al–N distances is that the impurity is in the surface plane, instead of occupying the center of the tetrahedral interstice.

The additional nitrogen atom in $Al_{44}N_2^+$ is adsorbed on top of the cluster surface, so it forms just three Al–N bonds. Notice that due to the mirror plane symmetry of the parent cluster, the second impurity might have occupied an equivalent cluster site as the first impurity, but in this way the separation between the two impurities would have been maximal. The doped system shows instead a strong preference toward segregation between a metallic host and an ionic molecular impurity, which compensates for the lower coordination of nitrogen. In fact, the calculated dynamical Born effective charges[64,65] for nitrogen atoms in the $Al_{44}N_2^+$ cluster are 2.7, the same as in the bulk limit.[63] This shows that the impurities have been fully reduced to form two nitrido anions. A corresponding analysis of the Born charges of Al atoms shows that the charge transferred to the impurity comes exclusively from its first atomic coordination shell, formed in this case by six Al atoms. The physical description of the charge-transfer process is essentially the same as recently reported for oxidized sodium clusters.[39] The average Al–N bond length in $Al_{44}N_2^+$ is 1.91 Å, and the N–N separation is 3.07 Å. Compared to the respective bulk values of 1.89 and 3.08 Å,[63] the results show that the impurity is almost a perfect fragment of the AlN crystal.

We have evaluated the energies involved in the "nitrogenation" reaction $Al_{44}^+ + N_2 \rightarrow Al_{44}N_2^+$ and the corresponding reaction for the metal cluster anion. The energies of the pure metal clusters are available from our previous work.[44,45] Both reactions are found to be exothermic at 0 K, with reaction excess energy values of 2.9 eV for the cation and 3.0 eV for the anion. The two values are quite similar because anion and cation share the same structure. The slightly higher exothermicity for the anion correlates with the local minimum of the electron affinity for Al_{44}^-,[45] which is thus more prone to transfer electrons to the impurity atoms.

We have also calculated the reaction excess energies at 900 K, where both pure and doped clusters are liquid-like. To this end, we have performed constant-temperature MD simulations with a thermalization stage of 50 ps and an additional length of 100 ps to calculate the time averages of the cluster energy. The bottom right plot in Figure 5 shows a typical atomic configu-

ration for the doped liquid cluster. During the simulation, the two nitrogen impurities remain close to each other, so the molecular impurity is not dissolved in the liquid cluster. The wetting of the molecular impurity is nevertheless more complete in the liquid phase: one of the two nitrido anions occupies a more internal position within the cluster, while the second one remains at the surface; each N atom is now on average coordinated to four aluminum atoms, so the net coordination of the impurities increases upon melting. The same structural trends were observed in oxidized liquid sodium clusters (see ref 38 for more complete details). Within our statistical accuracy, the excess energies are the same for both anion and cation in the liquid phase and lower by 0.75 eV as compared to the results at 0 K, so they compare quite reasonably with the experimental liquid dissociation energies of the order of 2.4 eV (see above). The reaction is significantly less exothermic in the liquid phase. This does not imply that the liquid clusters are less reactive than the solid clusters: we will see in the next section that the activation barrier for dissociation of N_2 is much lower for the liquid clusters, so the collision *kinetics* will make the liquid clusters more reactive even if the reaction is *thermodynamically* more favorable in the solid phase.

The GM structure of $Al_{43}N_2^{+/-}$ (not shown in Figure 5) is directly obtained from $Al_{44}N_2^{+/-}$ by removing one of the Al atoms with lowest coordination number. The calculated dissociation energy (loss of an Al atom) for $Al_{44}N_2^{+/-}$ is 3.5 eV, which is larger than the desorption energy (loss of N_2). At 900 K, the corresponding result is about 2.75 eV, which once more agrees very well with the liquid dissociation energies determined from the experiments. The theoretical results thus support the energy diagram shown in Figure 2. The liquid dissociation energies of $Al_{44}N_2^{+/-}$ are about 0.3–0.4 eV lower than the typical liquid values measured for pure aluminum clusters.[44,45]

It is interesting to compare the qualitative trend in the reaction excess energies with the one observed in oxidized sodium clusters.[38] The oxidation reaction was found to be more exothermic for liquid than for solid sodium clusters. This thermodynamically promotes the liquid phase and has the effect of systematically depressing the melting points and latent heats of melting of the doped clusters as compared to the corresponding values for pure sodium clusters. Exactly the opposite behavior is observed in N-doped aluminum clusters, so we expect the latent heats of the doped clusters to be larger than those of the pure aluminum clusters (this is a theoretical prediction which has not yet been tested experimentally). In oxygen-doped sodium clusters, the local atomic relaxation around the impurity puts the solid cluster under tensile strain, due to the rigidity of the solid phase. Upon melting, the strain is released because of the larger structural freedom of the liquid phase, which allows for a more complete optimization of the oxide/metal interface. This should be the general trend at the mesoscale and for sufficiently large clusters, for which the insoluble impurity represents just a small perturbation to the host metal, but obviously this is not the case for the small aluminum clusters considered here. In fact, in a previous study of Cu-doped aluminum clusters,[62] we have found that the doped clusters can have either smaller or larger latent heats than the pure metal clusters, depending on the specific cluster size, so the qualitative thermal behavior of the doped system is unpredictable in general for small clusters.

In order to better understand the distortion that the ionically bonded impurity induces on the metallic host cluster, we have calculated the average Al–Al bond length, the root-mean-square

(62) Saib, S.; Bokarissa, N.; Rodríguez-Hernández, P.; Muñoz, A. *Physica B* **2008**, *403*, 4059.
(63) Baroni, S.; de Gironcoli, S.; Dal Corso, A.; Giannozzi, P. *Rev. Mod. Phys.* **2001**, *73*, 515.
(64) Resta, R. *Rev. Mod. Phys.* **1994**, *66*, 899.
(65) Cao, B.; Starace, A. K.; Neal, C. M.; Jarrold, M. F.; Núñez, S.; López, J. M.; Aguado, A. *J. Chem. Phys.* **2008**, *129*, 124709.

Table 1. Average Al−Al Bond Length (*d*), Root-Mean-Square Deviation of the Al−Al Bond Lengths with Respect to the Average Value (Δ), and Average Radius (*r*) and Asphericity (β) of the Aluminum Host, Compared for Pure and Doped Clusters, Both in Their Solid and Liquid Phases[a]

	d	Δ	*r*	β
Al_{44}^+ (0 K)	2.81	0.07	4.29	0.13
$Al_{44}N_2^+$ (0 K)	2.82	0.09	4.30	0.14
Al_{44}^+ (900 K)	2.93	0.27	4.51	0.16
$Al_{44}N_2^+$ (900 K)	2.93	0.37	5.02	0.26

[a] All values are given in Å, except β which is adimensional. The γ values (see text) are not included because they do not provide any additional insight. The results for the corresponding anions are not shown either because they are qualitatively similar.

deviation of the Al−Al distances with respect to the average value (which provides a measure of the bond strain), and the average shape of the clusters as determined by their Hill−Wheeler parameters (*r*, β, and γ),[66,67] obtained from the three principal moments of inertia, $I_1 \geq I_2 \geq I_3$, as follows:

$$I_k = \frac{2}{3}r^2\left[1 + \beta \sin\left(\gamma + \frac{(4k-3)\pi}{6}\right)\right] \quad (2)$$

$$I_1 + I_2 + I_3 = 2r^2 \quad (3)$$

r is the root-mean-square radius of the cluster, β is a shape parameter quantifying its degree of asphericity, and γ quantifies its triaxiality. When calculating these parameters, we include only the aluminum atoms in the evaluation of the inertia tensors, and not the nitrogen atoms. This is because we want to analyze the distortion induced by the impurity on the host aluminum cluster. When calculating the average Al−Al distance, we consider that two Al atoms are connected if they are separated by less than 3.6 Å. This cutoff distance coincides with the first minimum in the liquid pair distribution function, which is the usual way of defining the radius of the first atomic coordination shell. The results are shown in Table 1. The introduction of the two nitrogen impurities hardly affects the average size and shape of the solid cluster. In particular, Δ remains almost the same upon doping, which implies that the impurity does not generate a significant strain within the host metal (there is negligible local relaxation around the impurity sites). In contrast, the structure of the liquid cluster is significantly perturbed by the dopant: first, its average radius increases by 11% because the whole cluster shape changes, becoming much less spherical (and so less compact) than for the pure liquid metal; second, even if the average Al−Al distance is not modified (as for the solid cluster), the Δ value increases by almost 40% upon doping, so the impurities increase the strain of the inherent liquid structures. Both factors contribute to make the reaction less exothermic in the liquid phase. The different sensitivity of solid and liquid aluminum clusters is probably due to the change in the relative strengths of Al−N and Al−Al bonds induced by heating: while the Al−N bond lengths are very similar at 0 and 900 K (bulk AlN melts at about 3000 K[68]), the Al−Al bonds are considerably weakened by the melting transition. As the cluster size is small, the whole liquid cluster structure is disrupted by the impurity. This is also the reason why the liquid dissociation energies (for

(66) Bulgac, A.; Kusnezov, D. *Phys. Rev. Lett.* **1992**, *68*, 1335.
(67) Bulgac, A.; Kusnezov, D. *Phys. Rev. B* **1992**, *45*, 1988.
(68) Goldberg, Y. In *Properties of Advanced Semiconductor Materials: GaN, AlN, InN, BN, SiC, SiGe*; Levinshtein, M. E., Rumyantsev, S. L., Shur, M. S., Eds.; John Wiley & Sons, Inc.: New York, 2001; pp 31−47.

loss of an Al atom) are much lower for the doped clusters than for the pure metal clusters.

2. Dissociation Pathway and Activation Energies. 2.1. Reproduction of the Experimental Results: MD Simulations of the Collision Process. Now that the thermodynamics of the chemisorption reaction are understood, we turn our attention to the collision dynamics. We have performed *ab initio* constant-energy MD simulations of the collision between N_2 and Al_{44}^+ (and Al_{44}^-) for four different initial temperatures of the metal clusters, namely 400, 500, 900, and 1000 K, and with a collision energy of 3.4 eV (which roughly corresponds to the measured kinetic energy threshold for the chemisorption reaction). Three independent runs were performed for each temperature and cluster charge when the N_2 molecule is oriented parallel to the cluster surface; six additional runs were performed when the N_2 bond is oriented perpendicular to the cluster surface, giving a total of 30 simulations.

A representative selection of the results obtained for the parallel orientation is shown in Figure 6. The two upper panels of Figure 6 show the time evolutions of the potential energy (left panel) and temperature (right panel) of the combined $Al_{44}^+-N_2$ system during the collision process, for two independent runs and with the solid metal cluster thermalized at 400 K. The temperature shown in Figure 6 is obtained from the total kinetic energy of the combined system through the equipartition theorem (i.e., $T = 2E/k_B$), so it includes the translational kinetic energy of the incoming N_2 molecule before the collision, and only represents an internal temperature after the doped cluster has formed. In both runs, the total potential energy initially decreases as the N_2 molecule approaches the metal cluster, reaching a minimum associated with a physisorbed state (see next section) where we position our zero of potential energy. The molecule then has to surmount a rather sharp collision barrier of approximately 3.4−3.5 eV, which is in reasonable agreement with the experimental threshold measurements. This barrier originates from the closed-shell electronic structure of the N_2 molecule (which has a huge HOMO−LUMO gap of 22.9 eV) and the associated Pauli repulsion between the overlapping electron density clouds of molecule and cluster. During the collision process, the N−N bond is steadily reduced and elongates up to an average value of 1.65 Å, and then the N_2 is embedded into the cluster surface, forming an activated complex with a temperature of about 600 K, that is, 200 K hotter than the original solid cluster. At this stage an analysis of the Born charges shows that the triple bond has been reduced to a single N−N bond, but the dissociation is not yet complete. The doped cluster remains in this activated state for some time, which we found to be shorter than 1 ps for some runs and as long as 10 ps in the least favorable run (not shown). The molecule then dissociates without an additional significant barrier (if there is a barrier, it is at most of the same order as the potential energy fluctuations, so it cannot be directly appreciated from Figure 6). In some runs (red curve in Figure 6), the potential energy decreases significantly after dissociation and the cluster temperature increases up to 750 K; a visual inspection of the MD trajectory reveals that the doped cluster remains in a hot solid phase. In other cases (black curve), the strong perturbation due to the high-energy impact and later N_2 dissociation induces a significant disorder in the host metal, so the doped cluster remains in a disordered cold phase. (Due to the limited time of the simulations, we cannot conclude if it is a cold liquid phase or just a high-energy amorphous isomer, because the doped cluster is not yet properly thermalized at the end of the
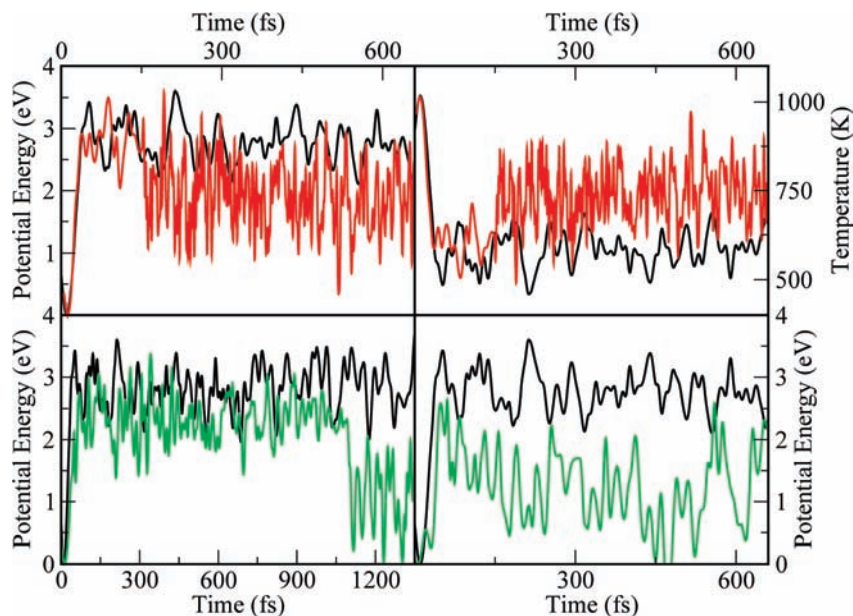
Figure 6. Top left: the time evolution of the potential energy for two independent constant-energy MD simulations of the collision between an N_2 molecule and an Al_{44}^+ cluster. In both cases the initial temperature of the cluster was 400 K. Top right: the time evolution of the temperature for the same two runs. Note that our temperature definition includes the translational kinetic energy of the incoming N_2 molecule before the collision. In the first simulation (black curve) the $Al_{44}N_2^+$ cluster remains in a cold disordered (or maybe liquid) phase after the collision; in the second one (red curve) the doped cluster remains in a hot solid phase. Bottom left: comparison of the potential energies during the collision of N_2 with a cluster cation (black curve) and a cluster anion (green curve), both at the same initial temperature of 400 K. Bottom right: comparison of the results for the collision with a solid Al_{44}^+ cluster at 400 K (black curve) and with a liquid Al_{44}^+ cluster at 900 K (green curve). The zero of potential energy is in all cases positioned at the first minimum of the graphs, corresponding to a physisorbed state (see text), so that one can directly read from the graphs an approximate value for the collision barriers.

simulations.) The potential energy and temperature are then almost unaffected after dissociation.

It is important to note that we position our reference zero energy at the energy of the physisorption minimum. Even if the initial kinetic energy is 3.1 eV, the potential energy of the $Al_{44}^{+/-}-N_2$ system initially decreases, and by the time the physisorption distance is reached, the relative kinetic energy is about 3.4 eV, of the same order of magnitude as the barrier surmounted. This means that we are really working close to threshold conditions at 400 K. In more detail, the surmounted barrier is found to be slightly larger than the relative kinetic energy. This means that not only the relative collision energy but also a small part of the cluster's initial thermal energy are converted into potential energy at the top of the barrier observed in the MD simulations.

Due to the rather limited number of runs and the significant thermal fluctuations, it is not easy to discern any clear trends about the detailed temperature dependence of the collision barriers from the MD simulations. Thus, the potential energy curves at 500 K (not shown) look rather similar to those at 400 K, which means that any difference in the activation barriers at 400 and 500 K is masked by the thermal fluctuations. However, comparing the potential energy curves for the cluster cation and anion at 400 K (bottom left panel in Figure 6), we systematically observe that the collision barrier for the anion is lower by 0.4−0.5 eV as compared to that for the cation. Similarly, a comparison of the potential energy curves at 400 (solid cluster) and 900 K (liquid cluster), shown in the bottom right panel of Figure 6, clearly shows that the collision barrier is significantly lower, by about 1 eV, in the liquid phase. Therefore, the dynamical simulations beautifully reproduce most of the experimental findings. The qualitative features of the collision process, namely the formation of an activated complex with a

single N−N bond before the final dissociation, are the same both for cation and anion, either solid or liquid.

When the N_2 molecular axis is perpendicular to the cluster surface, there are several possibilities regarding the specific site of the cluster surface on which the N atom lands: it can directly collide with an Al atom (on-top site), at the center of an Al−Al bond (bridge site), or at the center of the triangle formed by three Al surface atoms (hollow site). We have tried all these possibilities and observed that, at least at the simulated collision energy, the N_2 molecule always rebounds from the cluster and no dissociation occurs. The collision is inelastic, so the internal energy of the cluster is increased. Therefore, this is not an open channel for the chemisorption reaction under the conditions of the simulation. Although we have not tried any other orientations, intermediate between parallel and perpendicular, the present MD results suggest that the reaction will be easier as the orientation of the incoming N_2 molecule becomes closer to parallel.

2.2. Interpretation of Experimental Results: Constrained Geometry Optimizations. In order to get rid of the thermal noise inherent to a small number of short MD simulations, we have also performed a set of static calculations of the collision and dissociation processes, directed at obtaining a clearer picture of the trends as a function of cluster temperature and to assess the influence of the specific experimental threshold conditions (collision energies of 3.4 eV) on the obtained energy barriers. The static calculations involve constrained geometry optimizations in which the cluster−molecule separation is fixed at a number of values ranging from 0 to 4 Å, and where the molecule is oriented parallel to the cluster surface. We have compared the results of two constrained optimization schedules: in the first one, we allow for a complete relaxation of both aluminum cluster and N_2 molecule for each fixed cluster−molecule
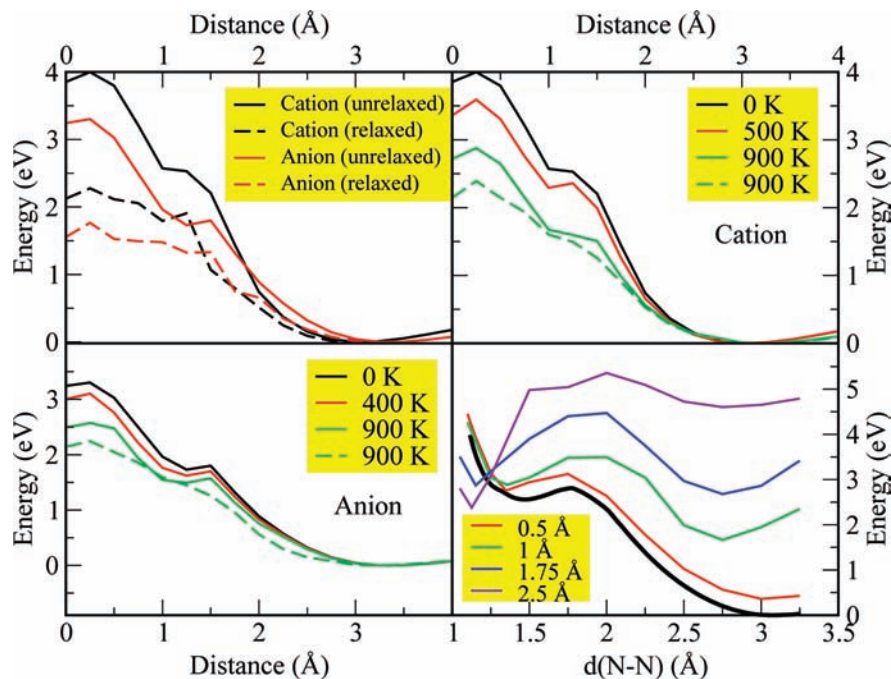
Figure 7. Top left: the dissociation potential energy curves for the cation (black lines) and the anion (red lines) at 0 K, as a function of the cluster−molecule separation. The dashed lines are obtained by allowing for a complete relaxation of the aluminum cluster at each cluster−molecule separation, while the solid lines are obtained by constraining the relaxation of the aluminum cluster so as to mimic the results of the MD simulations (see text for details). Top right and bottom left: the temperature dependence of the collision barriers for cation and anion clusters, respectively, as obtained from constrained relaxations. Two sets of results are shown at $T = 900$ K: in the first one (solid lines) the aluminum cluster preserves its solid-like geometry, but its lattice is expanded so as to match the correct liquid density at that temperature; in the second one (dashed lines), a typical liquid-like geometry is employed to model the collision. Bottom right: the variation of the potential energy with the N−N molecular distance at several fixed cluster−molecule separations. The thick black curve corresponds to the N_2 molecule embedded into the cluster surface, which is the possibility realized in the experiments.

separation. This schedule would correspond to the limit of an infinitely slow, parallel collision approach. In the second one, we try to mimic in a simple way the true experimental conditions by adding some more constraints. For this calculation to be meaningful, the added constraints should be few, simple, and physically motivated, that is, built upon the previous knowledge gathered in the MD simulations. An analysis of the MD trajectories shows that the N−N bond length steadily increases while approaching the metal cluster, but the cluster itself does not have time to relax in response to the incoming molecule when the collision energy is 3.4 eV, so the cluster is essentially frozen during the initial stages of the collision. Only when the nitrogen molecule is very close to the cluster surface (Al−N distances of the order of 1.8 Å) do the forces on some Al atoms become big enough for them to relax appreciably. Nevertheless, the velocities of those Al atoms during this final collision stage are just a small fraction (about 10%) of the velocity of the nitrogen atoms, so they never relax completely before the N_2 molecule is embedded into the cluster. The second optimization schedule is then chosen as follows: for cluster−molecule separations between 4 and 1.8 Å, the cluster is kept completely frozen; for shorter separations, those Al atoms which are in contact with the N_2 molecule are allowed to relax, but only up to a maximum displacement which is 10% of the molecule displacement. In practice, we have sampled the cluster−molecule separation at intervals of 0.2 Å, so in the final collision stage, the affected Al atoms are allowed to move a maximum of 0.02 Å for each cluster−molecule separation. The second schedule introduces thus two parameters: the critical Al−N distance which separates the initial and final stages of the collision, and the maximum displacement of Al atoms in the final stage. It is important to realize that by changing those two parameters one

might obtain very different values for the energy barriers, so we emphasize that we are not fitting those parameters to the experimental results but rather extracting them from a careful observation of the MD results. This is what makes the second optimization schedule sensible and meaningful.

A comparison of the two optimization schedules is shown in the upper left panel of Figure 7, for both cation and anion clusters in their zero temperature GM structures. In both runs, the N_2 molecule ends up embedded in the cluster surface, with an elongated N−N bond, as observed in the MD simulations. The collision barriers are, not surprisingly, lower in the fully relaxed runs, but the important point is that the effect is quantitatively very large. The barriers are as low as 2.3 eV for the cation and 1.8 eV for the anion, more than 1 eV lower than the experimentally determined barriers. In the unrelaxed runs, the barriers are 4.0 eV for the cation and 3.4 eV for the anion, which compare reasonably well with the extrapolations of the experimental results (Figure 4) to 0 K. There are two important implications to extract from this comparison. The first one is that the usual constrained static calculations, which search for the path with the lowest barrier by allowing for full atomic relaxation at each cluster−molecule separation, are not useful to interpret and reproduce the present experimental results. Instead, a fully dynamical simulation, incorporating the relevant experimental information, is mandatory. Only from such a simulation can one extract the additional constraints needed to model the experimental conditions via static calculations. The second one is of a practical nature: both the experimental and theoretical results suggest that the chemisorption reaction does not proceed under equilibrium conditions (in the simulations this is evident from the fact that the collision time, 60 fs, is shorter than a vibrational period). The short reaction time is a
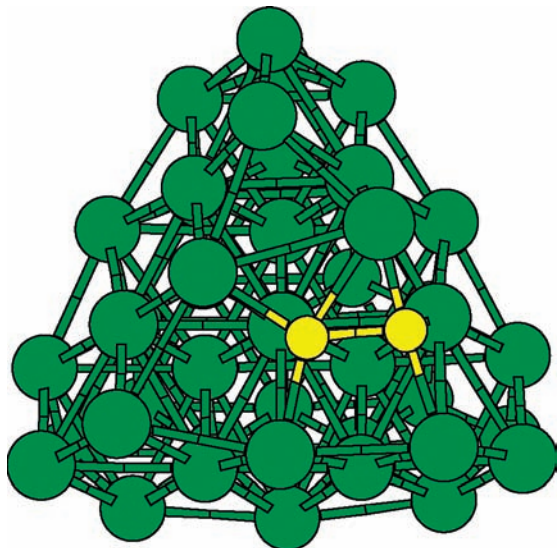
Figure 8. Metastable isomer formed after the collision, but before the full dissociation of the nitrogen molecule.

consequence of the high kinetic energy required to overcome the barrier. According to theory, it seems that the barrier against the reaction might be substantially lowered by working at a slower collision velocity, which might increase the reactivity rate by some orders of magnitude. But we are considering an activated process, so there must be a minimum collision kinetic energy below which the reaction is not possible. The experimental measurements show that the threshold energy is about 3 eV, so slower collisions are simply unreactive, and the limit barrier corresponding to an infinitely slow approach (dashed lines in Figure 7) is not realized in practice. In other words, the path with the lowest possible barrier is not dynamically accessible if the $Al_{44}^{+/-}-N_2$ system is isolated. This is an important conclusion, because it emphasizes in a very explicit way the need to consider the possible role of dynamical effects in the study of reactivity problems. The common practice of using static calculations to predict barrier heights will underestimate the barriers in cases where dynamic effects are important.

The energy values shown in the upper left panel of Figure 7 when the cluster−molecule separation is equal to zero do not correspond yet to a local minimum of the doped cluster, not even for the relaxed calculation, because the N_2 molecule and the cluster surface were forced to remain parallel. When a complete structural relaxation is performed, we obtain the metastable isomer shown in Figure 8, whose energy is approximately 0.5 eV below that of the physisorbed state. This complex is formed as an intermediate stage in the dissociation of the N_2. Its energy is more than 2 eV above that of the GM structure shown in Figure 5.

So the N_2 molecule does not completely dissociate at the end of the collision simulation. To complete the analysis of the dissociation process, we have performed an additional set of constrained static calculations. For each cluster−molecule separation, we have sampled different values of the N−N interatomic distance, in the range from 1.05 to 3.3 Å, allowing all the remaining degrees of freedom to relax. A representative subset of those results is shown in the bottom right panel of Figure 7 for the cation cluster (the results for the anion are qualitatively similar). Even for cluster−molecule separations as large as 2.5 Å, there are two local minima in the potential

energy, one corresponding to a bonded N_2 molecule and the other to a dissociated molecule. The bonded minimum steadily shifts from a value of $d(N-N) = 1.12$ Å at large cluster−molecule separations to a value of about 1.60 Å for the shortest cluster−molecule separation, this trend reflecting the progressive reduction of the two nitrogen atoms. The dissociated minimum is located at $d(N-N) = 3.1$ Å for short cluster−molecule separations and is shifted to 2.7 Å for long separations. The barrier against dissociation increases with the cluster−molecule separation, correlating with the degree of reduction of the nitrogen impurities: for the embedded impurity, there remains only a single bond between the nitrogens, so each of them already carries a substantial negative charge, and they strongly repel each other. Even if the dissociation involves some distortion of the host cluster (an animation showing the dissociation pathway is available in the Supporting Information), the N−N repulsion is so strong that the barrier is lower than 0.3 eV. This value is smaller than the potential energy fluctuations observed in the finite temperature MD runs, which demonstrates that the barrier observed in the experiments is substantially enhanced over the value due to the dissociation process alone by the dynamics of the reaction. For increasing cluster−molecule separations, the distortion of the host cluster is reduced, and at the same time the N−N bond is stronger, and the net result is an increase in the dissociation barrier. For cluster−molecule separations longer than 1.75 Å, the bonded minimum has a lower potential energy, while the opposite is true for cluster−molecule separations shorter than 1.75 Å. So in the limit of an infinitely slow approach and if equilibrium conditions hold, the molecule would dissociate before colliding with the cluster, with a combined barrier of about 2.8 eV. However, as mentioned above, this possibility may be very difficult to realize experimentally.

We have also employed constrained static optimizations to analyze the temperature dependence of the collision barrier with better resolution. To this end, we have first performed constant-temperature MD simulations for both Al_{44}^+ and Al_{44}^- at 400, 500, 900, and 1000 K. From these simulations we extract the average volume of the clusters at each temperature. Next, for the solid clusters at 400 and 500 K, we just take the perfect GM structure and homogeneously scale the atomic coordinates so as to match the atomic density appropriate to each finite temperature. The resulting structure is then employed in the simulation of the collision process, in exactly the same way as for the zero-temperature structure. A representative subset of these results is shown in the upper right (cation) and lower left (anion) panels of Figure 7, where we also reproduce the zero-temperature curves for the sake of a visual comparison. We clearly see that the theoretical reaction barriers decrease upon heating the solid cluster: the cation barrier is 3.6 eV at 500 K, and the anion barrier is 3.1 eV at 400 K. Not only the relative magnitude of the barrier for cation and anion, but also the experimental observation that the temperature dependence of the anion barrier is smaller than the cation one, are properly reproduced by the calculations. Thus, theory suggests that the main reason for the higher reactivity of hotter solid clusters is just thermal expansion, which obviously weakens the Al−Al bonds. The atomic disorder coming from the thermal motion (not included in the static calculations) is, at most, of secondary importance.

Motivated by these observations, we have performed two different optimization runs for the high temperatures where the clusters are liquid. In the first one (solid line in Figure 7), we employed once more the perfect solid GM structure, but

expanded so as to match the typical liquid densities at 900 and 1000 K. In the second one (dashed line in Figure 7), we properly employed a liquid configuration extracted from the MD runs. In the first run, the cation barrier at 900 K is already reduced to 2.85 eV, while the anion barrier is 2.55 eV. Although still higher than the experimental barriers at 900 K, these results show that the largest contribution to the much higher reactivity of the liquid phase comes just from the volume change of melting. The barriers obtained in the second run are 2.37 eV for the cation and 2.28 eV for the anion, which compare quite well with the corresponding experimental values. In particular, in the liquid phase, the reactions of the cation and anion have roughly the same kinetic energy thresholds. A comparison of the two runs separates the relative contributions of atomic density and atomic disorder to the collision barriers.

The volume change of the cluster affects the activation barrier through changes in both the electronic and the geometric structures. Thermal expansion is known to affect the electronic properties of metal clusters. For example, the polarizabilities increase markedly with temperature,[69] implying that the electrons are more sensitive and respond more to external perturbations when the ionic lattice is expanded. This electronic effect lowers the initial Pauli repulsion and facilitates electron transfer from the aluminum cluster to the N_2 molecule. The structure (separation between the aluminum atoms) is also important: once the electron transfer (and ionic-like Al−N bonding) starts, an expanded lattice exerts a larger force along the internuclear axis of N_2, tending to separate the two atoms and further reducing the barrier. This is a simple structural or epitaxial effect.

Conclusions

We have presented a combined experimental and theoretical study of the reaction of dinitrogen with an $Al_{44}^{+/-}$ cluster as a function of cluster temperature. The most abundant collision product at all but the highest cluster temperatures and relative kinetic energies is $Al_{44}N_2^{+/-}$, where the dinitrogen molecule has been chemisorbed onto the metal cluster. The cross sections for chemisorption show a threshold energy, indicating that it is an activated process. The threshold energies show a smooth decrease with cluster temperature within both solid and liquid phases, and a stronger and sudden decrease by around 1 eV at the melting point, so there is a very large increase in the cluster reactivity upon melting. Above the threshold, the cross sections increase with the relative kinetic energy, plateau, and then start decreasing. The decrease occurs because the chemisorption product dissociates when it is highly excited at high relative collision energies and high initial temperatures. The fit to the region where the cross sections roll-over and decrease allows us to extract values for the dissociation energies of the chemisorption product.

Density functional calculations have been employed to obtain the putative global minimum structure of the reactants and the $Al_{44}N_2^{+/-}$ products. The "nitrogenation" reaction is found to be exothermic with an excess reaction energy of 3 eV at 0 K (solid phase) and of 2.25 eV at 900 K (liquid phase). This is in

excellent agreement with the $D(N_2)$ values (the binding energy of N_2 to the cluster) deduced from the experiments for the liquid phase (2.37 eV for the cation and 2.46 eV for the anion). The calculated dissociation energy of $Al_{44}N_2^{+/-}$ (loss of one aluminum atom) is 3.5 eV at 0 K and about 2.75 eV in the liquid phase. Again, this is in good agreement with the values deduced from the experiments, where we find $D(Al)$ is 2.64 eV for the liquid cation and 2.67 eV for the liquid anion.

When the N_2 is oriented parallel to the cluster surface, dissociative chemisorption is observed in the simulations. As the N_2 approaches the metal cluster, the potential energy of the combined $Al_{44}^{+/-}-N_2$ system initially decreases and reaches a minimum associated with a physisorbed state; it sharply increases upon further approach, with a maximum barrier height of about 3.4 eV, and then the molecule is embedded into the cluster. The N−N bond length steadily increases as the cluster−molecule distance decreases, reaching a value of about 1.65 Å just before it collides with the surface. At this point the nitrogen molecule has been partially reduced but is not yet fully dissociated. This complex persists for a few picoseconds before the N_2 molecule finally dissociates, without an appreciable additional barrier. At the end of the process, the cluster is approximately 200 K hotter than before the collision, so solid cluster reactants may be found in the liquid phase after the collision. The simulations properly reproduce reasonable values for the energy barriers surmounted under the experimental conditions, as well as their temperature dependence. The decrease in the threshold energies upon heating the cluster has been shown to be mainly due to the thermal expansion of the cluster, while the strong increase in reactivity upon melting is related both to the volume change of melting and to atomic disorder.

The theoretical results suggest that the barrier for chemisorption might be substantially lowered by working at slower collision velocities. But the experimental results clearly show the presence of a threshold relative kinetic energy, below which no reaction occurs. In practice this suggests that the path with the lowest possible barrier found in the constrained calculations is not dynamically accessible. At the high collision energies needed to observe the reaction, the metal cluster has not enough time to adapt its structure to the incoming N_2 molecule. Full dynamical calculations are therefore needed in order to interpret the experimental measurements.

Supporting Information Available: Animation file (.xyz) showing the dissociation of the N_2 molecule, corresponding to the bottom right panel of Figure 7, and details of the computational settings employed in this study. This material is available free of charge via the Internet at http://pubs.acs.org.

(69) Kummel, S.; Akola, J.; Manninen, M. *Phys. Rev. Lett.* **2000**, *84*, 3827.

JA103356R